Heterogeneous Drying of Colloidal Polymer Films: Dependence on Added Salt

ARTICLE *in* LANGMUIR · AUGUST 2008

Impact Factor: 4.46 · DOI: 10.1021/la800525n · Source: PubMed

4 AUTHORS, INCLUDING:

Joseph Keddie
University of Surrey
147 PUBLICATIONS **3,830** CITATIONS

SEE PROFILE

Heterogeneous Drying of Colloidal Polymer Films: Dependence on Added Salt

Alexander M. König,[†] Tecla G. Weerakkody,[‡] Joseph L. Keddie,*[,‡] and Diethelm Johannsmann*[,†]

Institute of Physical Chemistry, Clausthal University of Technology, Arnold-Sommerfeld-Str. 4, D-38678 Clausthal-Zellerfeld, Germany, and Department of Physics, Faculty of Engineering and Physical Sciences, University of Surrey, Guildford, Surrey GU2 7XH, United Kingdom

Received February 18, 2008. Revised Manuscript Received April 10, 2008

Using magnetic resonance profiling coupled with dynamic light scattering, we have investigated the mechanisms leading to the formation of a partly coalesced surface layer, or "open skin", during film formation from waterborne polymer dispersions. We present the first use of the skewness of the distribution of free water as a model-free indicator of the spatial nonuniformity of drying. The skewness reaches a maximum at the same time at which a strong, static component, presumably originating from a skin at the film/air interface, appears in the light scattering data. Addition of salt to the dispersion increases both the skewness of the distribution of free water and the propensity for skin formation. Surprisingly, the drying is influenced not only by the concentration and valency of the ions in the salt but also by the particular ion. At intermediate particle densities, added salt strongly lowers the cooperative diffusion coefficient, D_{coop}. When the particles reach close packing, D_{coop} sharply increases. If the particles readily coalesce, the effects of the increased diffusivity will be counteracted, thereby inducing the formation of a skin. A modified Peclet number, *Pe*, using D_{coop}, is proposed, so that the presence of salt is explicitly considered. This modified *Pe* is able to predict the nonuniformity in drying that leads to skin formation.

Introduction

The formation of polymer films from waterborne polymer dispersions is a process of ever-increasing practical relevance.[1–3] A major driving factor is the compliance with environmental regulations, which severely limit the amount of volatile organic compounds (VOCs) that can be released into the atmosphere upon drying. Film formation is commonly divided into three stages, which are the evaporation of water leading to particle packing (stage I), particle deformation to fill all available volume (stage II), and interdiffusion across particle/particle boundaries, that is, coalescence (stage III). During the first stage, water evaporates until the particles come into contact. Subsequently, the particles deform as the interstitial water is eliminated. Finally, any surfactant membranes break so that polymer chains from neighboring particles interdiffuse, thereby producing a homogeneous, tough film.

As has been frequently emphasized, film formation usually proceeds in a spatially heterogeneous way.[1] Heterogeneity occurs both in the plane of the film[4,5] (i.e., edge-in drying) and perpendicularly to the substrate[6,7] (i.e., top-down drying). The time at which water recedes from a film's edge has been demonstrated experimentally to be proportional to the reduced capillary pressure.[5] Edge-in drying can be prevented by blowing hot air across the film surface. Vertical gradients in water concentration can never be entirely avoided because these gradients drive the transport of water toward the film surface. However, the extent and consequences of vertical gradients in water concentration vary considerably. If particles are packed together at the film/air interface and if the particles are subject to wet sintering (being highly deformable), then a process model developed by Routh and Russel (R−R model) predicts coalescence to create a so-called "skin" layer above a wet layer.[6,8,9] There is clear experimental evidence for the development of skin layers.[10,11]

In applications, skin formation is usually considered to be a serious problem. Water transport by diffusion *through* a coalesced polymer layer is slower than flow along particle/particle boundaries.[12] Experiments have shown that a skin layer on a latex film traps water beneath it, thereby slowing down the drying process.[13] Subsequently, trapped water will reduce the film's mechanical strength and adhesion.[14] Furthermore, as drying proceeds, the skin might rupture or wrinkle, which will result in an irregular surface.[15] For these various reasons, the topic has attracted intense interest.

Simulations predict that colloidal particles will accumulate at the surface of thick films undergoing relatively fast drying.[16] Cryogenic scanning electron microscopy (SEM) images of films that were quenched during the process of drying have provided

* To whom correspondence should be addressed. E-mail: johannsmann@pc.tu-clausthal.de (D.J.); j.keddie@surrey.ac.uk (J.L.K.). Telephone: +49 5323-72 3768(D.J.); +44 1483-686803(J.L.K.). Fax: +49 5323-72 4835 (D.J.); +44 1483-686781 (J.L.K.).

[†] Clausthal University of Technology.

[‡] University of Surrey.

(1) Keddie, J. L. *Mater. Sci. Eng., R* **1997**, *21*, 101–170.
(2) Steward, P. A.; Hearn, J.; Wilkinson, M. C. *Adv. Colloid Interface Sci.* **2000**, *86*, 195–267.
(3) Winnik, M. A. *Curr. Opin. Colloid Interface Sci.* **1997**, *2*, 192–199.
(4) Routh, A. F.; Russel, W. B. *AIChE J.* **1998**, *44*, 2088–2098.
(5) Salamanca, J. M.; Ciampi, E.; Faux, D. A.; Glover, P. M.; McDonald, P. J.; Routh, A. F.; Peters, A.; Satguru, R.; Keddie, J. L. *Langmuir* **2001**, *17*, 3202–3207.
(6) Routh, A. F.; Russel, W. B. *Ind. Eng. Chem. Res.* **2001**, *40*, 4302–4308.
(7) Gorce, J. P.; Bovey, D.; McDonald, P. J.; Palasz, P.; Taylor, D.; Keddie, J. L. *Eur. Phys. J. E* **2002**, *8*, 421–429.
(8) Routh, A. F.; Russel, W. B. *Langmuir* **1999**, *15*, 7762–7773.
(9) Guigner, D.; Fischer, C.; Holl, Y. *Langmuir* **2001**, *17*, 3598.
(10) Sheetz, D. P. *J. Appl. Polym. Sci.* **1965**, *9*, 3759.
(11) Mallégol, J.; Bennett, G.; Dupont, O.; McDonald, P. J.; Keddie, J. L. *J. Adhes.* **2006**, *82*, 217.
(12) Van der Wel, G. K.; Adan, O. C. G. *Prog. Org. Coat.* **1999**, *37*, 1.
(13) Erkselius, S.; Wadsö, L.; Karlsson, O. J. *J. Colloid Interface Sci.* **2008**, *317*, 83.
(14) Yang, Y.-K.; Li, H.; Wang, F. *J. Adhes. Sci. Technol.* **2003**, *17*, 1741.
(15) Brochard-Wyart, F.; de Gennes, P. G. *Science* **2003**, *300*, 441–441.
(16) Routh, A. F.; Zimmerman, W. B. *Chem. Eng. Sci.* **2004**, *59*, 2961.

10.1021/la800525n CCC: $40.75
Published on Web 06/19/2008

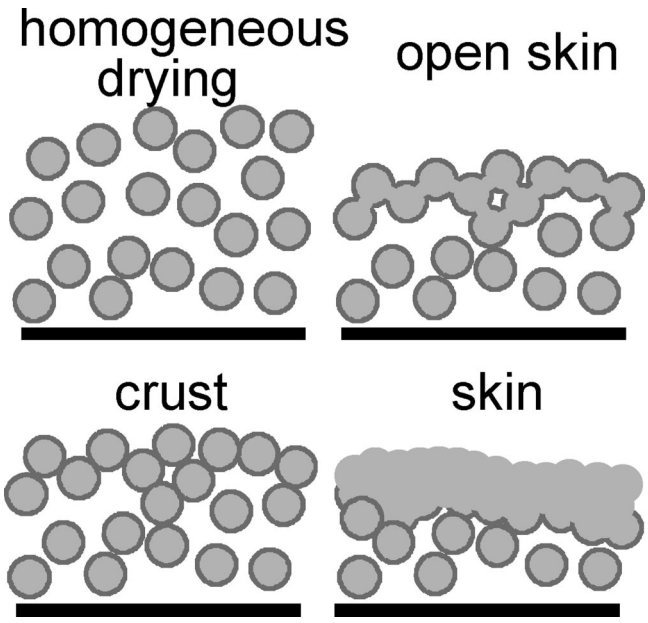

Figure 1. Sketches of various forms of homogeneous or heterogeneous drying. The dark lines denote the surfactant membranes separating the particles.

impressive evidence to support this view.[17] In these images, one can clearly see particles being accumulated at the top of the film. Metaphorically speaking, the air/water interface acts like a snow plow, piling up particles just below the phase boundary. Pileup is prevented if the recently created concentration gradients quickly equilibrate via diffusion. The competition of pileup and diffusion has been put into quantitative terms in a dimensionless parameter, called the Peclet number, *Pe*.[6,8] The *Pe* is the ratio of two characteristic time scales, which are the time needed to diffusively equilibrate gradients in particle concentration and the time of drying. For a film of initial thickness, H_0, with water evaporation leading to the surface receding at a speed, *E*, *Pe* can be most simply expressed as H_0E/D_0, where D_0 is the Stokes−Einstein diffusion coefficient. Particle accumulation occurs whenever the speed of drying exceeds the rate by which concentration gradients decay. This condition corresponds to $Pe \gg 1$. Recent experimental evidence[18] shows that the water concentration gradient in the vertical direction is proportional to $Pe^{0.8}$, which compares to a prediction of $Pe^{0.5}$ (ref 16). Note, however, that the Stokes−Einstein law only holds in the dilute limit. A drawback of basing the calculation of *Pe* on the Stokes−Einstein diffusivity is that this equation does not account for particle/particle interactions.

A second prerequisite for skin formation within the R−R model is a sufficiently high deformability of the particles, so that they can form a continuous layer while the material underneath is still wet. More specifically, there is a second dimensionless number, $\bar{\lambda}$, which compares the time scale of particle deformation to the time scale of drying. One has $\bar{\lambda} = \eta_0 aE/(\gamma_{wat}H_0)$ with η_0 being the zero shear-rate viscosity of the polymer particles, *a* being the particle radius, and γ_{wat} being the surface energy of the air/water interface. For $Pe > 1$ but $\bar{\lambda} \gg 1$, particles will be in close contact at the film surface, so that they are elastically coupled, but they will not be coalesced. A so-called "crust" will be formed, as illustrated in Figure 1.

In order to explore skin formation in colloidal dispersions, we have simultaneously applied magnetic resonance profiling (MRP)[19,20] and diffusion wave spectroscopy (DWS)[21] to drying polymer films. There have been limited previous applications of light scattering techniques to studies of film formation,[22,23] and there are no previous reports of MRP and DWS being used together in such a study. MRP yields the volume fraction of mobile water as a function of the distance from the substrate, $\varphi_w(z)$. Skin or crust formation is thereby indicated by a step in $\varphi_w(z)$ along the vertical direction, corresponding to a higher polymer concentration near the surface. DWS yields the mobility of particles inside the film. Given the complicated geometry in experiments on drying films, the particle self-diffusion coefficient cannot be quantitatively derived from the autocorrelation function (ACF). Still, one can compare different data sets and determine any differences in particle mobility. In addition to the particle mobility, light scattering contains an essential second bit of information, which is the amplitude of the autocorrelation function. Should a skin form at the top of a film, it will act as a static scatterer. This strong background is superimposed onto the dynamic fluctuations of scattering from the bulk that is still mobile at this time, which lowers the amplitude of the ACF.

A previous study by Erkselius et al.[13] has provided the first significant evidence that electrostatic stabilization influences the drying rate and total drying time of latex films. In our research reported herein, salt was added to the dispersions in order to vary the interparticle forces. The influence of salt is threefold: First, salt screens the electrostatic repulsion, thereby widening the local cages of confinement around the particles and allowing for faster Brownian motion. The short-time self-diffusion coefficient of the particles increases. Second, electrostatic screening lowers the osmotic pressure of the particles and thereby the thermodynamic driving force for the equilibration of concentration fluctuations. Third and importantly, salt can induce particle aggregation ("salting-out") in the late stages of drying by reducing the barrier to aggregation.[24] In ref 13, *faster* drying has been attributed to the presence of salt, when particle flocculation at higher ionic concentrations caused sedimentation and the avoidance of a skin layer.[13]

The evolution of a concentration profile in colloidal dispersions is governed by the cooperative diffusion coefficient, D_{coop} (also called "mutual diffusion coefficient"). The relation between D_{coop} and D_0 (valid at infinite dilution) can be rather complex. We provide an estimate in the Discussion section. When particles strongly repel each other (for instance, due to electrostatic interaction), the equilibration of concentration gradients speeds up considerably because of cooperative motion. D_{coop} must not be confused with the self-diffusion coefficient, which governs Brownian motion. In situations where individual particles cannot leave the local cages because the packing is too high, cooperative motion along the concentration gradients will still occur. At moderate concentrations, where the particles interact, but are not yet close-packed, D_{coop} is much greater than D_0 if the particle surfaces are charged. The effect of charge on D_{coop} is reduced by the addition of salt in the continuous medium.

It is also relevant to note that the tendency of ions to "salt-out" colloidal particles is poorly understood. The tendency for different ions to influence colloidal stability can be placed in a well-

(17) Ma, Y.; Davis, H. T.; Scriven, L. E. *Prog. Org. Coat.* **2005**, *52*, 46–62.
(18) Ekanayake P.; McDonald P. J.; Keddie J. L. To appear in *European Physical Journal: Special Topics*.
(19) Glover, P. M.; Aptaker, P. S.; Bowler, J. R.; Ciampi, E.; McDonald, P. J. *J. Magn. Reson.* **1999**, *139*, 90–97.
(20) McDonald, P. J.; Newling, B. *Rep. Prog. Phys.* **1998**, *61*, 1441–1493.
(21) Weitz, D. A.; Pine, D. In *Dynamic Light Scattering*; Brown, W., Ed.; Oxford University Press: New York, 1992.
(22) Schmidt, M.; Krieger, S.; Johannsmann, D. *Prog. Colloid Polym. Sci.* **1997**, *104*, 191.
(23) Narita, T.; Beauvais, C.; Hebraud, P.; Lequeux, F. *Eur. Phys. J. E* **2004**, *14*, 287–292.
(24) Israelachvili, J. N. *Surface and Intermolecular Forces*; Academic Press: New York, 1991.

defined order called the Hofmeister series.[25,26] The Hofmeister series cannot be explained merely by electrostatic screening as described by the Derjaguin−Landau−Verwey−Overbeek (DLVO) theory, which considers the valency of the ions. Numerous properties of electrolyte solutions (including protein aggregation, the speed of chemical reactions, catalytic activity of enzymes, surface tension, the critical micelle concentration, and others) depend on the type of the dissolved ions, and the dependency follows the order of the Hofmeister series.[26] The fact that so many diverse properties all lead to the Hofmeister series suggests that there is a general mechanism underlying these different manifestations. The operative mechanism is still under debate. The ion's tendency to stabilize or destabilize the water structure around it has been regarded as a key factor. Recently, however, this notion has been questioned,[27,28] and dispersion forces have been put forward as an alternative explanation.[29]

A recent study[28] has shown that the order of the ions in the Hofmeister series can be correlated with their tendency to disorder alkyl chains in fatty acid layers at interfaces. We speculate that Hofmeister effects could also contribute to the destabilization of surfactant bilayers at particle/particle interfaces. We note that the R−R model[8] assumes that any surfactant membranes readily rupture when the particles come into contact, and the effects of salt are not considered. Hence, ion effects are not predicted by the model and could yield otherwise unexplainable results.

Materials and Experimental Protocol

An acrylic latex was prepared by miniemulsion polymerization. A copolymer was polymerized from butyl acrylate and methyl methacrylate in a 1:1 weight ratio, using an anionic surfactant (Dowfax 2A1). A mixture of ammonium persulfate and sodium metabisulfate was used as the initiator. These initiators impart a negative charge to the particle surfaces, which with the charge of the surfactant imparts an electrostatic stabilization. The average particle diameter, according to dynamic light scattering measurements, was 180 nm. Atomic force microscopy (AFM) images show that the size distribution is not monodisperse. Polydispersity slightly increases the volume fraction of close packing (cf. eq 26). Otherwise, it is unessential. The initial solids content was 47 wt %. The glass transition temperature was determined to be $T_g \sim 18$ °C by differential scanning calorimetry. Using the densities of $\rho_{PMMA} = 1.19$ g/cm^3 and $\rho_{PBA} = 1.03$ g/cm^3, one derives an initial solids content by volume of $\Phi_0 = 43$ vol %. The addition of excess NaCl to the latex resulted in coagulation, indicating that the latex was charge stabilized.

Electrolyte solutions were freshly prepared from the following salts: Na_2SO_4, $NaNO_3$, $NaClO_4$, and $MgCl_2$. $MgCl_2$ was chosen because it is very strongly destabilizing. The three other salts share a common cation. The anions differ in their precipitating power according to the Hofmeister series ($SO_4^{2-} < NO_3^- < ClO_4^-$). In order to have the same solids content in all experiments, a fixed volume of 1 mL of the particular salt solution was added to a 5 mL volume of the dispersion in each experiment. We chose two ionic strengths in the aqueous phase of the dispersion: 238 and 119 mmol/L. After dilution with the salt solution, Φ_0 was 36 vol %. It is relevant to note that the dispersions containing $MgCl_2$ at an ionic strength of 119 mmol/L were marginally stable. All other dispersions showed good stability.

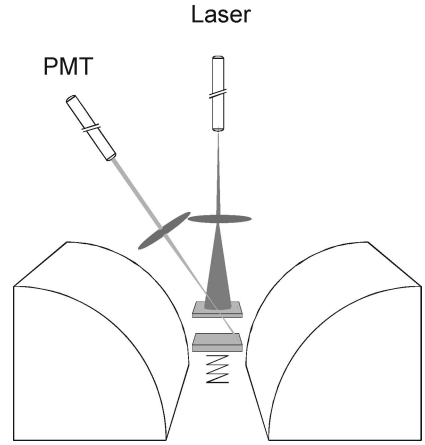

Figure 2. Sketch of the experimental setup. The sample is situated in a strongly heterogeneous magnetic field. The NMR spectrometer acquires profiles of the free water $\varphi_w(z)$ at a rate of about 1 data trace per 2 min. In parallel, the particle mobility is monitored from the top by diffusion wave spectroscopy.

Magnetic Resonance Profiling. Magnetic resonance profiling and its application to the drying of polymer dispersions have been described in the literature.[7,19] Briefly, the drying film is situated in a magnetic field gradient that is normal to plane of the substrate (Figure 2). The local field strength encodes the height above the substrate, and NMR signals can be separately acquired in horizontal cuts through the depth of the sample.

Wet films were cast onto clean glass coverslips (2 cm × 2 cm) and immediately placed in the magnet at a position corresponding to a magnetic field strength of 0.7 T and a field gradient strength of 17.5 T m^{-1}. The initial film thickness, H_0, was typically 600 μm. The temperature within the magnet was ∼25 °C for all experiments, and the air above the sample was static. The room humidity was typically 40%. Previous work has shown that, in the static air within the instrument, the evaporation rate is limited by the diffusion of water in the vapor phase. Therefore, any variations in humidity have a negligible effect on the evaporation rate.

Signals were obtained using a quadrature echo sequence:[20] 90_x-τ-$(90_y$-τ-echo-τ-$)_n$ for $n = 32$ echoes and a pulse gap of $\tau = 95.0$ μs. To obtain a profile, the echoes were Fourier-transformed and then summed, thus giving an NMR signal intensity profile as a function of vertical position. No significant signal is observed from the polymer phase, and the water spin−spin relaxation time is largely independent of the polymer concentration in the dispersion. Hence, the NMR intensity is a fair measure of the water content that can be calibrated from the time-zero data with a known, uniform concentration. The pixel resolution in these experiments was about 15 μm. Due to its reliance on the spin−spin relaxation time, the instrument only probes "free" (i.e., nonbound) water. A film, which is dry in the sense of MRP, may still contain tightly bound water that is not detected by the instrument. With regard to skin formation, free water is a more relevant parameter than the total amount of water because free water allows for fast mass transport and reflects the volume fraction of interstitial voids.

Figure 3 shows three sets of water distribution profiles. In these profiles, water concentration is presented on the vertical axis. The vertical position in a film, which is measured as the distance from the interface with the substrate, is presented on the horizontal axis. In this way, the top of the film is represented at the right-hand side of the profile. A series of profiles from the same sample is presented over time running along the third axis. Time zero is defined as the start of the experiment.

The experiment shown in Figure 3a was conducted on a dispersion with no added salt. The NMR signal intensity does not vary much with vertical position in the film, indicating that the distribution of water is rather homogeneous throughout the entire drying process. In the experiment shown in Figure 3b, $MgCl_2$ had been added to the dispersion at an ionic strength of 119 mmol/L. Figure 3c shows a

(25) Hofmeister, F.; Naunyn-Schmiedebergs, F. *Arch. Pathol. Lab. Med.* **1888**, *24*, 247.
(26) Kunz, W.; Lo Nostro, P.; Ninham, B. W. *Curr. Opin. Colloid Interface Sci.* **2004**, *9*, 1–18.
(27) Batchelor, J. D.; Olteanu, A.; Tripathy, A.; Pielak, G. J. *J. Am. Chem. Soc.* **2004**, *126*, 1958.
(28) Gurau, M. C.; Lim, S.-M.; Castellana, E. T.; Albertorio, F.; Kataoka, S.; Cremer, P. S. *J. Am. Chem. Soc.* **2004**, *126*, 10522.
(29) Boström, M.; Williams, D. R. M.; Ninham, B. W. *Phys. Rev. Lett.* **2001**, *87*, 168103.

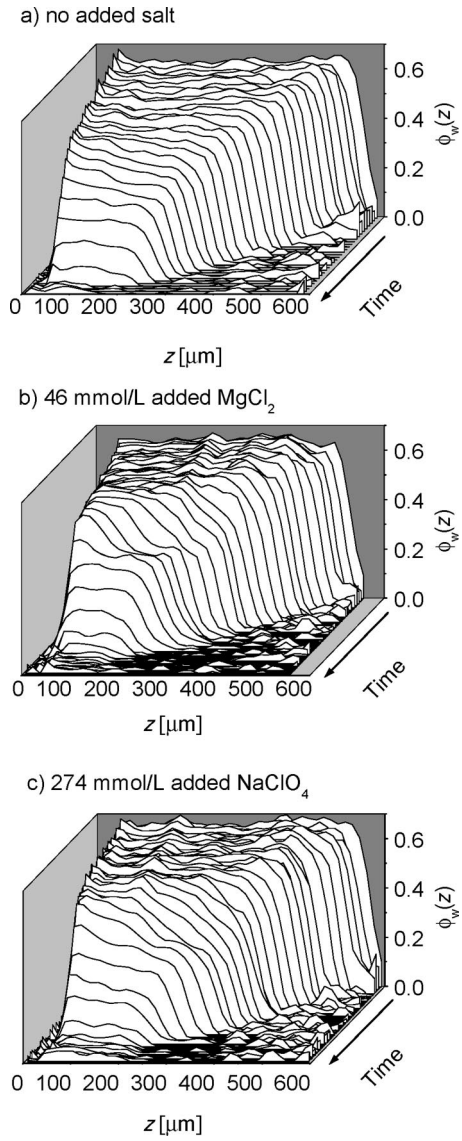

Figure 3. Series of distributions $\varphi_w(z)$ acquired in the presence of added salt at regular intervals throughout the entire drying time (shown in the third dimension). The NMR intensity on the vertical axis is proportional to $\varphi_w(z)$. Panel (a) shows the reference experiment on the latex applied as received. For this case, the distribution is rather symmetric throughout the entire process of drying. Addition of $MgCl_2$ at 119 mmol/L and $NaClO_4$ at 238 mmol/L increases the asymmetry (panels b and c, respectively). At later times in (b) and (c), there is a step in $\varphi_w(z)$, separating the skin and the dilute dispersion below.

data set from an experiment where Na_2SO_4 was added to the dispersion at an ionic strength of 238 mmol/L. In the experiments shown in parts b and c of Figure 3, the water distribution developed an asymmetric shape. Drying proceeded heterogeneously.

In order to describe the influence of added salt on skin formation, a quantitative indicator of vertical heterogeneity is needed. We use the skewness of the profile $\varphi_w(z)$ for that purpose. The analysis comprised the following steps:

(a) Normalization. To correct for the sensitivity decline over the film thickness, profile intensities were normalized by dividing by the profile obtained from an elastomer standard. In a second step, the profiles were divided by the function $A - Bz$, where the parameters A and B were chosen such that the first profile of any given experiment had a flat top at $\varphi_w(z) = 1 - \Phi_0$. This step served to normalize the profiles and to remove a slight residual slope in the profiles, which was still present after the first normalization step. The second step assumes a uniform distribution of water at the start of the experiment.

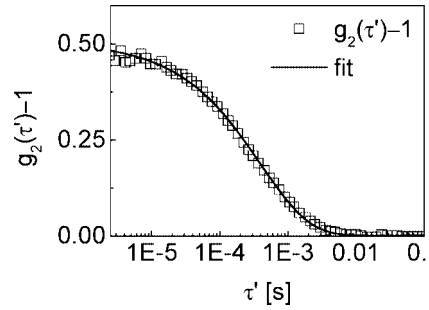

Figure 4. Typical autocorrelation curve of the scattered light. The line is a fit with the function $A \exp(-(\tau'/\tau_D)^\beta)$.

(b) Smoothing. An adjacent average according to $\varphi_i \rightarrow 1/4(\varphi_{i-1} + 2\varphi_i + \varphi_{i+1})$ was applied. This step removed a systematic even-odd difference between adjacent data points. This artifact is related to insufficiently accurate pulse sequences of the NMR spectrometer.

(c) Calculation of the Integral Amount of Free Water. The amount of free water is the integral of $\varphi_w(z)$ over the full range of z. For the purpose of integration, we have cut all profiles to $\varphi_w(z) = 0$ when $\varphi_w(z)$ fell to below the noise level. Otherwise, the calculations of higher moments (see below) would have been strongly affected by the noise. The noise level was found to increase with increasing distance from the substrate. Therefore, we used the function $\varphi_{noise} = \alpha z^2$ with $\alpha \sim 6 \times 10^{-6}\ \mu m^{-2}$ as the "noise level".

(d) Calculation of the Skewness. The skewness is a measure of the asymmetry of a profile. It is thus a model-free estimator of heterogeneous drying. Positive skewness (a "right-skewed profile") implies a tail or a pedestal extending to the right (i.e., to the film/air interface). The skewness is defined as

$$S = \frac{m^*}{(m_2^*)^{3/2}} \tag{1}$$

with $m_3^* = m_3/m_0$ and $m_2^* = m_2/m_0$ being the normalized third and second moments of the distribution, respectively. The nth moment of any given discrete distribution $\varphi_i(z_i)$ is given by

$$m_n = \sum z_i^n \varphi_i \Delta z \tag{2}$$

The sum runs over all data points. For the calculation of moments, the origin of the z-scale was set such that the first moment vanishes (i.e., all z_i values are to be understood as distances to the center of gravity of the profile). Once again, the profiles were cut off when $\varphi_w(z)$ fell below the noise level.

(e) Calculation of the Solids Content. The vertically averaged solids content, $\langle\Phi(t)\rangle$, was calculated via the relation

$$\langle\Phi(t)\rangle = 1 - \frac{m_0(t)}{m_0(0)}(1 - \Phi_0)\frac{H_0}{H(t)} \tag{3}$$

where $m_0(t)$ is the zeroth moment of $\varphi_w(z)$ at time t, $m_0(0)$ is the zeroth moment at $t = 0$, Φ_0 is the solids content at $t = 0$, $H(t)$ is the thickness at time t, and H_0 is the initial thickness. The thickness, $H(t)$, was determined from the MRP profiles. In doing so, we assumed that the upper edge of the water profile coincides with the upper edge of the film. That would not be true if there were a dry, open layer at the top, containing no free water at all. Such a dry surface seems unlikely, especially in the earlier stages of drying. Also, if this were the case, one would expect an extended tail in $\varphi_w(z)$ at some intermediate stage in drying (which was not observed). Note that the time derivative of $H(t)$ is not strictly equal to the water evaporation speed, E, because the samples were affected by the so-called coffee-stain effect.[30] That is, some material moved from the center of the film toward the rim (not probed in the MRP experiment), thereby decreasing the measured film thickness in the center for reasons other than water evaporation.

Diffusing Wave Spectroscopy. In order to monitor particle mobility in parallel to the water content, a diffusing wave spectroscopy (DWS) setup was installed above the MRP instrument. Briefly, a HeNe laser illuminated the sample from the top. Scattered light was collected from the center of the film by means of an optical fiber equipped with a collimator. The light was fed into a photon correlation spectroscopy (PCS) module. Autocorrelation functions were acquired at a rate of three data traces per minute. The autocorrelation functions were fitted with stretched exponentials of the form

$$g_2(\tau') - 1 = A \exp\left(-\left(\frac{\tau'}{\tau_D}\right)^{\beta}\right) \quad (4)$$

where A is an amplitude, τ_D is a decay time, and the exponent $\beta < 1$ is an indicator of nonexponentiality. Figure 4 shows a typical autocorrelation curve and a fit. In DWS, β cannot be quantitatively translated into dynamical heterogeneity (coexistence of fast and slow dynamics) because the path length distribution introduces a distribution of decay times even if the medium of interest would yield a single exponential in conventional light scattering. Actually, β was found to decrease with drying time in the present work. This matches the expectation of an increasing dynamical heterogeneity as the sample dries from the top to the bottom. With regard to skin formation, the amplitude of the autocorrelation function, A, is the prime parameter of interest. An amplitude much less than unity provides evidence for the presence of static scatterers. In this regard, DWS works in essentially the same way as conventional dynamic light scattering.

Results and Discussion

We first discuss crust formation as evidenced by the DWS data. Figure 5 shows that, for a latex containing added salt, the amplitude of the autocorrelation function sometimes sharply drops during an experiment. We refer to the time at which this happen as T_S. The corresponding solids content, Φ_S, is indicated with a vertical line in Figure 5. Simultaneous MRP shows that water is present in the surface layer, indicating that full coalescence has not created a skin. The drop in amplitude is caused by the (rather sudden) appearance of a static scattering component in the DWS data. A drying latex film is a spatially heterogeneous medium, where solidified and liquid components may coexist. We associate the drop in amplitude with the formation of a solidified layer at the top, which is best described as a crust (Figure 1) until proven otherwise. (As we will discuss later, the surface layer has not coalesced fully to create a skin.) The light scattered from these assemblies of elastically coupled particles fluctuates at a time scale longer than one second. The decay time of the autocorrelation function, τ_D, goes to infinity (or, more precisely, leaves the experimental window) soon after T_S. The time stretch during which a crust coexists with a liquid underneath is rather short. Particle diffusion comes to rest a few minutes after the crust has formed.

Interestingly, the crust moves laterally even after Brownian motion has stopped. One can visually observe this movement when imaging the drying film with a camera. The lateral drift of the scatterers causes a rather sizable variability of the scattering intensity (i.e., the count rate as determined by the PCS module) on a time scale of minutes (encircled region in Figure 5). These fluctuations slow down with continued drying. They almost come to rest at the same time at which the free water has disappeared from the film according to the MRP data. Some limited scattering still persists even after drying is complete because the film surface is rough.

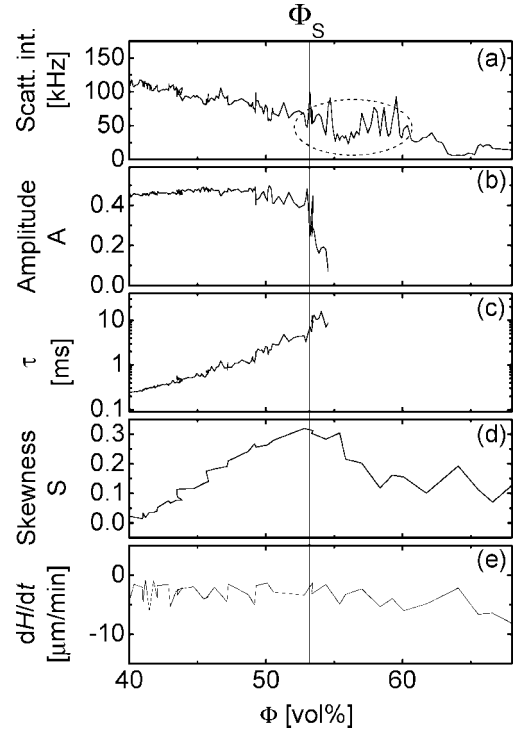

Figure 5. Typical DWS/MRP data set. This particular latex film contained $MgCl_2$ at an ionic strength of 119 mmol/L. (a) Count rate of the DWS instrument, which is a measure of turbidity. The turbidity does not decrease to zero because the surface remains rough after drying. The dotted circle shows noise attributed to the lateral drift of a "skin layer." (b) Amplitude of the autocorrelation function, A. The amplitude sharply drops at the time where a static scatterer (a skin) forms at the film surface. (c) Autocorrelation time τ_D. τ_D increases with drying time, reflecting the slowing down of Brownian motion. (d) Skewness of water distributions, $\varphi_w(z)$, obtained from MRP. (e) Drying rate, dH/dt. The skewness peaks at about the same at which the skin develops. The vertical line shows the vertically averaged solids content at which a solidified layer appears at the top of the film, Φ_S. The drying rate remains about constant after the solidified layer appears.

As the comparison between the MRP results and the DWS data shows, there is a strong correlation between the skewness of the water distribution and crust formation (Figure 5), as detected via DWS. The crust is created when the skewness is at its maximum. The maximum of the skewness occurs when the vertically averaged particle volume fraction is around 54%. The numerical value of this *average* should not be overinterpreted: Φ is higher than 54% inside the dry layer at the top and lower in the fluid range below. Still, the maximum in skewness is expected at a solids content where the sample solidifies. For hard, monodisperse spheres, this solids content is in the region of 55%.

Figure 6 shows the amplitude of the autocorrelation function, A, the decay time τ_D, the skewness of the water distribution, and the drying rate dH/dt for films containing one of three different salts and for the as-received latex without added salt for a reference sample. The ionic strengths of added salts were chosen such that the value of the Debye screening length, κ^{-1}, in the dispersion was about 0.5 nm, taking the effects of the different valencies (1 or 2) into account.[24] As water evaporates, the salt concentration increases and κ^{-1} decreases, accordingly. For the reference sample, κ^{-1} is much larger than 0.5 nm because the electrolyte concentration is naturally lower. The exact value of κ^{-1} is not known because both the surfactant and the initiator are charged and the degree to which these components are dissolved in the serum is not known.

(30) Deegan, R. D.; Bakajin, O.; Dupont, T. F.; Huber, G.; Nagel, S. R.; Witten, T. A. *Nature* **1997**, *389*, 827–829.

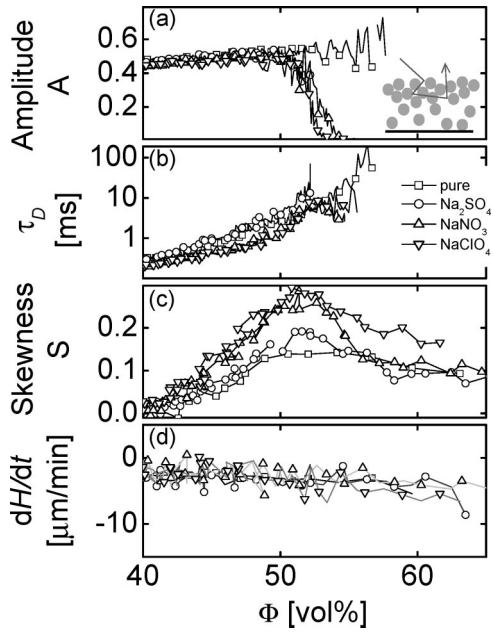

Figure 6. Comparison of the influence of three different types of salts. The increase in ionic strength due to the addition of salt was 238 mmol/L in all cases. For $NaNO_3$ and $NaClO_4$, one finds skin formation, while a skin does not form for Na_2SO_4 and for the pure dispersion. Correlating well to this finding, the skewness is highest for $NaNO_3$ and $NaClO_4$. In the initial part of the drying, the autocorrelation time slightly decreases upon the addition of salt. This can be explained as a reduction in the local caging. DWS mostly probes motion on the local scale, which is governed by the short-time self-diffusion coefficient. This parameter increases as the electrostatic interaction is reduced.

Evidence for a crust layer was found in the DWS data when drying dispersions containing $NaNO_3$ and $NaClO_4$, whereas no such layer was found for the as-received latex and for the sample containing Na_2SO_4. The former two samples have a significantly higher skewness than the latter (Figure 7).

The R−R model in its standard form does not explain why the addition of salt increases the water nonuniformity. In the Stokes−Einstein limit, the diffusivity is not influenced by interparticle forces. Even if the Stokes−Einstein diffusivity is replaced by a cooperative diffusion coefficient (see below), it is not clear why an ion's position in the Hofmeister series should affect the diffusivity. On the other hand, particle coalescence and the rupture of surfactant membranes, in particular, *are* among the properties following the Hofmeister series. This suggests that membrane rupture induced by added salt aids the development of heterogeneity and possible skin formation.

Estimation of the Peclet Number. In order to more quantitatively describe the role of interparticle potentials in the skin formation process, we estimate the Peclet number for the films investigated in this study, taking interactions into account. Interactions enter the Peclet number via cooperative diffusion. Within the standard picture, crust layers (which can then lead to skin formation) will only develop when $Pe \gg 1$. *Pe* is defined as the ratio of the time scale at which concentration differences diffusively decay, τ_{diff}, to the characteristic drying time, τ_{dry}, such that

$$Pe = \frac{\tau_{diff}}{\tau_{dry}} = \frac{H_0^2/D_{coop}}{H_0/E} = \frac{EH_0}{D_{coop}} \quad (5)$$

In our work, E is obtained from dH/dt, also taking into account lateral flow (see Appendix A). In a departure from previous work, we propose the use of D_{coop} rather than D_0 in the expression

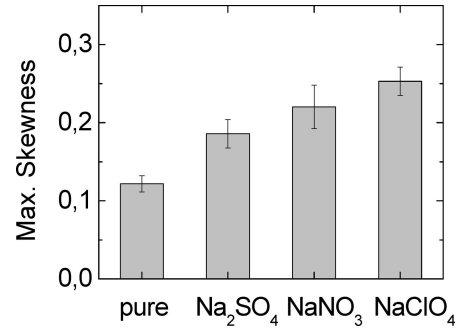

Figure 7. Maximum skewness averaged over three experiments for the pure dispersion and dispersions containing Na_2SO_4, $NaNO_3$, and $NaClO_4$ at an ionic strength of 238 mmol/L.

for *Pe*. D_{coop} is defined via Fick's first law ($J = -D_{coop}\nabla c$, with J being the flow and c being the concentration). In the dilute limit, the cooperative diffusion coefficient (governing concentration gradients) is equal to the self-diffusion coefficient (governing Brownian motion and the mean-square displacement of individual particles, $\langle \Delta r^2 \rangle$, via $\langle \Delta r^2 \rangle = 6D_{self}t$). Strictly speaking, diffusion should be described as "noncooperative" in the dilute limit. For particles of radius a in a continuous medium with a viscosity of μ, both are given by the Stokes−Einstein formula $D_0 = k_BT/(6\pi\mu a)$, with T being the absolute temperature and k_B being the Boltzmann constant. At higher concentrations, hydrodynamic interactions as well as static interparticle forces come into play. Usually, these slow down the motion of individual particles (for instance, by caging).[31] At the same time, they speed up the equilibration of concentration distributions via cooperative motion. More quantitatively, we have[32]

$$D_{coop} = D_0\, K(\Phi)\,(1-\Phi)\frac{4\pi a^3}{3}\frac{1}{k_BT}\left(\frac{d\Pi(\Phi)}{d\Phi}\right) \quad (6)$$

$K(\Phi)$ is the sedimentation coefficient, accounting for the fact the hydrodynamic backflow is slowed down by the neighboring particles, and $\Pi(\Phi)$ is the osmotic pressure. We expand on the meaning of the cooperative diffusion coefficient in Appendix B. The sedimentation coefficient can be approximated as[33]

$$K(\Phi) \sim \frac{1 - \frac{3}{2}\Phi^{1/3} + \frac{3}{2}\Phi^{5/3} - \Phi^2}{1 + \frac{2}{3}\Phi^{5/3}} \quad (7)$$

Equation 7 is the analytical solution of a cell model. A spherical particle was assumed to be contained in a second spherical volume with frictionless walls. Φ is the ratio of the two volumes. For the purpose of this estimate, we identify the parameter Φ with the solids content. In the range of solids content of interest here ($\Phi = 0.4-0.65$), $K(\Phi)$ decreases from 0.04 to 0.01. Equation 7 shows that $K(\Phi)$ decreases with increasing solids content.

The osmotic pressure, $\Pi(\Phi)$, has three contributions, which originate from electrostatic repulsion, van der Waals attraction, and entropy. We therefore have the three corresponding terms in the expression for Π:[32,34]

$$\Pi(D) \sim \frac{\sqrt{6}}{A_h}(F_{ES}(D) + F_A(D)) + p_{entr} \quad (8)$$

where A_h is the surface of interaction. We approximate A_h as the

(31) McPhie, M. G.; Nagele, G. *J. Chem. Phys.* **2007**, *127*, 034906.
(32) Bowen, W. R.; Mongruel, A. *Colloids Surf., A* **1998**, *138*, 161–172.
(33) Happel, J.; Brenner, H. *Low Reynolds Number Hydrodynamics*; Kluwer: Norwell, MA, 1973.
(34) Bowen, W. R.; Jenner, F. *Chem. Eng. Sci.* **1995**, *50*, 1707–1736.

surface of a sphere with radius $a + D/2$, that is, $A_h \sim 4\pi(a + D/2)^2$. D is the mean distance between particle surfaces, and it is related to Φ via the relations

$$\frac{\Phi}{\Phi_{RCP}} \sim \frac{a^3}{(a+D/2)^3} \sim \frac{a^3}{a^3+3Da^2}$$

$$D \sim \frac{a}{3}\left(\frac{\Phi_{RCP}}{\Phi} - 1\right) \quad (9)$$

$\Phi_{RCP} \sim 63$ vol % is the solids content at random close-packing. We assume that the particles are hard enough to remain spherical at this solids content. Softer spherical particles would deform and coalesce upon first contact. The parameter F_{ES} in eq 8 is the electrostatic force between two charged spheres. For the purpose of this estimate, we assume a 1:1 electrolyte and use the weak overlap approximation,[24] leading to

$$F_{ES} \sim \frac{\pi a\ 64\ k_B T \rho_\infty}{\kappa}\left(\tanh\left(\frac{e\Psi_0}{k_B T}\right)\right)^2 \exp(-\kappa D)$$

$$= \pi a\ 0.0482\ [\text{electrolyte}]^{1/2}\left(\tanh\left(\frac{\Psi_0[mV]}{103}\right)\right)^2 \times \exp(-\kappa D) \quad (10)$$

Here, Ψ_0 is the electrical potential at the particle surface and ρ_∞ is the electrolyte concentration far away from charged surfaces. A typical value for particles stabilized with a sulfonate-based surfactant is $\Psi_0 \sim -80$ mV. Measurements of the zeta potential on the dispersions used in this study are consistent with this value. As pointed out earlier, $\kappa^{-1} = 0.5$ nm in the dispersion at the salt concentrations used. In general, κ is given by

$$\kappa^2 = \left(\frac{\sum \rho_{\infty i} e^2 z_i^2}{\varepsilon\varepsilon_0 k_B T}\right) \quad (11)$$

where the index i runs over all ionic species, z is the valency, $\rho_{\infty i}$ is the concentration (in ions per m^3) far away from charged surfaces, ε is the relative dielectric permittivity of the liquid, and ε_0 is the dielectric permittivity of vacuum. Note that $\rho_{\infty i}$ increases when water evaporates so that κ^{-1} decreases during drying. This effect was taken into account in the calculations presented later. However, whereas in the study by Erkselius et al.[13] the particles became unstable because of the rise in ionic concentration during drying, our calculations indicate that the critical coagulation concentration (CCC) is not reached in our system until *after* the time at which particle close-packing occurs.

The van der Waals force between spherical particles is given by[35]

$$F_A = -\frac{dV_A}{dD}$$

$$V_A \sim -\frac{A_H}{6D}\left[\frac{2a^2}{D^2+4aD} + \frac{2a^2}{(D+2a)^2} + \ln\left(1 - \frac{4a^2}{(D+2a)^2}\right)\right] \quad (12)$$

A_H is the Hamaker constant. Using $A_H \sim (A_{pol}^{1/2} - A_w^{1/2})^2$ and further using $A_{pol} \sim 8.2 \times 10^{-20}$ J and $A_w \sim 3.7 \times 10^{-20}$ J,[36] we arrive at $A_H \sim 0.9 \times 10^{-20}$ J.

For the entropic pressure, we follow eq 12 in ref 37. The relation is explicit but somewhat lengthy. Inserting numbers, one finds that p_{entr} is small compared to the electrostatic pressure unless one considers a solids content near to the point of particle close-packing. At $\Phi \sim 0.74$, p_{entr} sharply diverges. The upper range of solids contents is not considered here because coalescence will modify the picture.

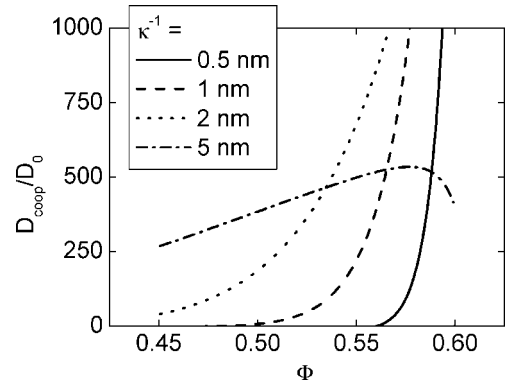

Figure 8. Cooperative diffusion coefficients calculated according to eqs 6–12. The input parameters are $\Psi_0 = -80$ mV, $A_H = 0.9 \times 10^{-10}$ J, and $a = 90$ nm. For $\kappa^{-1} > 2$ nm (corresponding to ionic strength of 23 mmol/L), the D_{coop} is about a factor of 100 higher than the Stokes−Einstein value, D_0. It depends on concentration.

Using eqs 6–12, one can estimate D_{coop} and its dependence on solids content and added salt. The result of this estimate is shown in Figure 8. The particle volume fraction, Φ, has been limited to $\Phi < 60\%$ because the model does not account for coalescence. Coalescence must enter the picture at around the point of particle close-packing. The input parameters to the calculation are the particle radius, a (determined by DLS as 90 nm), the surface potential, Ψ_0 (−80 mV), and the Hamaker constant, A_H (as chosen above). Note that this model does not differentiate between different types of ions with the same valency. The only input parameters into the DLVO theory are the surface potential, the ions' valencies, the ionic strength, and the particles' Hamaker constant.

Consider first the case of a Debye length larger than 2 nm. This would correspond to the reference experiments conducted without added salt. For these cases, the cooperative diffusion coefficient is much larger than the Stokes−Einstein value and weakly depends on Φ. This is a consequence of the fact that electrostatic repulsion softens the interparticle potential. D_{coop} may decrease at close-packing due to the van der Waals attractions. The value of D_{coop} is more than 100 times greater than D_0. Inserting the Stokes−Einstein value $D_0 = k_B T/(6\pi\mu a)$ and using a viscosity of $\mu = 1$ mPa s (corresponding to water), D_{coop} comes out to be around 10^{-5} cm^2/s. Inserting this value into eq 5 and further using $H_0 \sim 6 \times 10^{-2}$ cm as well as a drying time of $\tau_{dry} \sim 8100$ s, we arrive at the following estimate for *Pe*:

$$Pe = \frac{\tau_{diff}}{\tau_{dry}} \sim \frac{H_0^2}{D_{coop}}\frac{1}{\tau_{dry}} \sim \frac{(6\times10^{-2}\text{cm})^2}{(10^{-5}\text{cm}^2/\text{s})}\frac{1}{8100\text{ s}} \sim 0.04 \quad (13)$$

For $Pe < 1$, particle accumulation at the film surface is not expected according to the R−R argument. Particle accumulation is a prerequisite for crust formation. Indeed, a crust is not observed in our experiments without added salt, which is consistent with $Pe \sim 0.04$.

At a Debye length of 0.5 nm, the situation is changed. At $\Phi \sim 0.5$, D_{coop} is about equal to the Stokes−Einstein value, D_0. Inserting this value into eq 13, we find $Pe \sim 4$, which would predict nonuniform drying and particle accumulation at the film surface, as was observed experimentally with the addition of salt. A lowered value of D_{coop} at the same time implies a faster motion on the local scale. Because the interparticle repulsion has been reduced relative to the experiments without added salt, the particles feel the caging by their neighbors to a lesser extent. The

(35) Bowen, W. R.; Jenner, F. *Adv. Colloid Interface Sci.* **1995**, *56*, 201–243.
(36) Kaneda, I.; Vincent, B. *J. Colloid Interface Sci.* **2004**, *274*, 49–54.
(37) Hall, K. R. *J. Chem. Phys.* **1972**, *57*, 2252.

short-time self-diffusion coefficient therefore increases. DWS is mostly sensitive to the variability of next-neighbor distances. These fluctuate faster if the repulsion is reduced. The autocorrelation time in the DWS data, τ_D, therefore decreases (Figure 6b).

However, even in the presence of added salt, D_{coop} sharply increases as the particle volume fraction, Φ, approaches 0.6. The added salt screens the electrostatic interactions at distances larger than the Debye length, but at short distances the electrostatic interaction is still strong. Observe that eq 10 contains the square root of the electrolyte concentration in the numerator. When the particles approach closely, the osmotic pressure of the counterions in the gap becomes very large.

The consequences for the drying process are the following. At moderate concentrations ($\Phi \sim 0.5$), *Pe* is larger than one and particles therefore accumulate at the top. The snow plow effect is active. However, the Peclet number inside the densified layer sharply increases and particles will still escape skin formation because they are driven away from the film/air interface once the local solids content approaches 0.6. Moreover, if particles are sufficiently stable against coalescence, skin formation will not occur under these conditions. However, at $\Phi \sim 0.6$, the particles have approached closely and coalescence is imminent. Importantly, the data indicate that the rate of coalescence depends on the type of ion employed. Coalescence is among the phenomena affected by an ion's position in the Hofmeister series.

Addition of ions affects the skewness in two ways. First, it will (always) induce vertical heterogeneity because it will decrease D_{coop}. Second, the ions may encourage coalescence (and thereby further increase the skewness), if the respective ions are destabilizing. We checked for the destabilizing action of Na_2SO_4, $NaNO_3$, and $NaClO_4$ by determining the critical coagulation concentrations (CCCs), which were 2.7, 0.96, and 0.94 mol/L for Na_2SO_4, $NaNO_3$, and $NaClO_4$, respectively. The CCC is lowest for $NaClO_4$, which also induces the largest skewness in drying.

It is interesting to compare the estimates of D_{coop} derived using eqs 6–12 to experimental values derived from the profiles, $\varphi_w(z)$, and Fick's first law ($J = -D_{coop}\nabla c$). Note that, for binary, incompressible systems, D_{coop} is always the same for both components, and we can obtain D_{coop} from the evolution of $\varphi_w(z)$. Both the flow rate of water toward the surface, J, and the gradient of water concentration, ∇c, can be extracted from experiments. The calculation of the flow rate from $\varphi_w(z, t)$ is provided in Appendix A. One has

$$\frac{J_w}{\rho_w} = -\frac{1}{(1-\bar{\varphi}_w)}\frac{dm_{0,w}}{dt} + \left(\frac{\bar{\varphi}_w}{(1-\bar{\varphi}_w)} - \varphi_w(H)\right)\frac{dH}{dt} \quad (14)$$

where ρ_w is the density of water and $\bar{\varphi}_w$ is the vertically averaged water content.

First, consider the experiment shown in Figure 3a, which did not show crust or skin formation. At a drying time of $t = 100$ min, the analysis yields $\bar{\varphi}_w \sim 40\%$, $\varphi_w(H) \sim 37\%$, $dm_{0,w}/dt \sim -3.8\ \mu$m/min, $dH/dt \sim -2.9\ \mu$m/min, $dc/dz \sim 5.2 \times 10^8$ g/m^4, and $D_{coop} \sim 1.7 \times 10^{-6}$ cm^2/s (Figure 9a). Using $\tau_{dry} \sim 8100$ s and $H_0 \sim 5.5 \times 10^{-2}$ cm, we estimate the Peclet number as *Pe* ~ 0.2 (eq 14). Crust formation is therefore not predicted. As a second example, consider the experiment shown in Figure 3b, which *did* show crust formation. At a drying time of $t = 102$ min, we have $\bar{\varphi}_w \sim 46\%$, $\varphi_w(H) \sim 34\%$, $dm_{0,w}/dt \sim -3.6\ \mu$m/min, $dH/dt \sim -2.8\ \mu$m/min, $dc/dz \sim 1.9 \times 10^9$ g/m^4, and $D_{coop} \sim 4.6 \times 10^{-7}$ cm^2/s (Figure 9b). Using $\tau_{dry} \sim 8520$ s and $H_0 \sim 5.2 \times 10^{-2}$ cm, we estimate the Peclet number as *Pe* ~ 0.7. Although crust formation is *not* predicted by this *Pe*, the expected increase in *Pe* is observed compared to the first example. The same kind of analysis leads to *Pe* ~ 0.7 for the experiment shown in Figure 3c. Clearly, the addition of salt did slow down cooperative diffusion, but the effect amounts to a factor of less than 4, while eqs 6–12 predicted a factor of around 100. Presumably, the discrepancy can be attributed to elastic contacts between particles touching each other. Once the particles have partly coalesced, these contacts again increase the cooperativity of particle movement. We further elaborate on the dynamics of this elastic network in the following section.

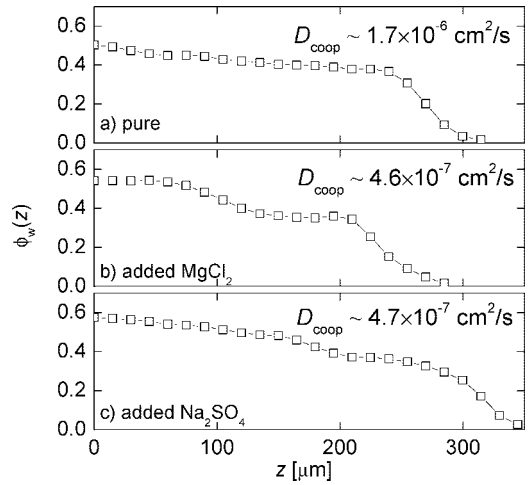

Figure 9. An estimate of the cooperative diffusion coefficient can be based on the concentration gradient and the vertical flow rate of water. The profiles correspond to the experiments shown in Figure 3 ($t = 100$ min, 102 and 102 min for the top to the bottom panel, respectively).

Estimation of Particle Viscosity and Particle Deformation Rate. In order to model the evolution of $\varphi_w(z)$ at concentrations beyond the volume fraction of the glass transition of $\Phi_{gl} \sim 53$ vol %, one would need to include the elastic forces inside the network of (randomly packed) contacting spheres. Particles will pack in a crust at the top of the film during drying without actually forming a skin. Two cases have to be distinguished. The particles may remain entirely separate. This case would, for instance, happen with high-T_g materials or with those that are very well stabilized against aggregation. A second case is partial coalescence. This would typically happen with harder particles (at a temperature just above the T_g) which are not well stabilized against aggregation. When such particles touch, the surfactant membranes break and the sintering process is initiated. However, the sintering is so slow that the water channels do not actually close before drying is complete.[38] Such a layer might be called an "open skin" (Figure 1). Below, we argue that the films investigated here develop such an open skin.

We do not attempt a description of the transition regime, where there is a loosely coupled elastic network still experiencing electrostatic repulsion. However, once the elastic network has become so dense that particle deformation dominates the film formation kinetics, the R−R model again applies. Particle deformation limits the speed of film formation if the particles are sufficiently hard. Since the T_g of the films formed here is around 18 °C, particle deformation is expected to be slow. In passing, we note that a model based on foam drainage applies in the opposite limit of soft spheres.[39]

The R−R model uses the terminology of viscoelasticity, and we follow that usage. Note, however, that one might, in principle, also add a term describing the negative isotropic pressure exerted

(38) Kiil, S. *Prog. Org. Coat.* **2006**, *57*, 236.
(39) Narita, T.; Hebraud, P.; Lequeux, F. *Eur. Phys. J. E* **2005**, *17*, 69–76.

by coalescence into eq 8, thereby staying within the conceptual frame of eqs 6–12. This negative pressure is the consequence of cohesion. For densely packed spheres, the R−R model relates the rate of drying to the viscosity of the particles. Skin formation only occurs if the particles are sufficiently soft. Otherwise, the particles do not form a dense layer. As already noted, particle deformability is described by a dimensionless parameter $\bar{\lambda} = \eta_0 aE/(\gamma_{wat} H_0)$. As we show in Appendix C, $\bar{\lambda}$ can be deduced from $\varphi_w(z, t)$ via

$$\bar{\lambda} = \frac{7}{5} \frac{\bar{\gamma}\langle\Phi\rangle^2}{\Phi_{RCP}\tau_{dry}} \left(\frac{\partial\Phi}{\partial t}\right)^{-1} \tag{15}$$

This relation assumes that deformability limits the rate of compaction. The parameter $\bar{\gamma}$ is the ratio of the particle/water interfacial tension and the air/water interfacial tension, which was assumed to be 0.5 in this estimate. The volume fraction at close-packing, Φ_{RCP}, is taken to be 63 vol %. Analyzing the time stretch between $t = 80$ min and $t = 105$ min, we find a $\bar{\lambda}$ value in the region of 0.5 for the data sets shown in Figure 3. Within the R−R model, this value of $\bar{\lambda}$ suggests that compaction is driven either by wet sintering or by capillary forces.[6]

Given that $\bar{\lambda}$ is close to 1, we conclude that the layer formed at the top is not a closed film (a "skin" in the narrow sense of the word). The same conclusion is reached from Figures 5e and 6d. Whereas there is clear evidence of a static scatterer at volume fractions above Φ_S, the rate of evaporation dH/dt does *not* slow down after the elastic layer has formed. Water channels remain open, because the particle deformation rate is small. Moreover, noting that the experimental temperature of ∼25 °C is within approximately 7 °C of the polymer's T_g, the R−R process model[8] does not predict wet sintering, thus preventing skin formation. An "open skin" (see Figure 1) is expected and is consistent with experimental observations.

Results reported by Erkselius et al.[13] contain a result which is a counterexample to our findings. They find that the addition of salt (but not so much as to induce sedimentation) leads to a *closed* skin as indicated by a decrease in evaporation rate. The T_g of their latex was 18 °C, which is identical to ours. One would expect therefore that $\bar{\lambda}$ is similar in both sets of experiments and hence the tendency to create a closed skin would likewise be identical. The fact that our latex films did not create a closed skin layer is likely to be the result of subtle effects of particle packing and the stabilizing effect of the surfactant in resisting particle coalescence. Neither of these effects is considered explicitly in the R−R model.

Conclusions

Applying magnetic resonance profiling and diffusion wave spectroscopy simultaneously in the same experiment, we have investigated the vertical heterogeneity of the water distribution and possible skin formation in drying polymer dispersions. Using the two techniques together provides a complete picture of the surface layer with information on both the particle dynamics (coupling) *and* the composition. We proposed the use of the skewness of the profile $\varphi_w(z)$ as an indicator of heterogeneity. The skewness peaks at a vertically averaged solids content of around 54 vol %, which is close to the volume fraction where hard-sphere colloids go through the glass transition. At the same solids content, one sometimes observes a strong static component in the scattering, which originates from a crust layer.

Addition of salt increases the skewness and the likelihood of subsequent skin formation. The strength of the effect depends on the particular type of ion. These results suggest that the destabilizing effect of the ions on the surfactant membranes separating the particles promotes heterogeneous drying. The order in which the ions influence destabilization is suggestive of a Hofmeister effect. In turn, both the speed of particle diffusion and the rate of coalescence have an influence on skin formation. Particle accumulation during drying was successfully predicted by a Peclet number that considered the cooperative particle diffusion rather than the standard Stokes−Einstein diffusivity. Whereas maps of the relevant film formation mechanisms predicted by the standard R−R model[6] employ the latter definition of the Peclet number, our results reveal the importance of considering cooperative effects. As the R−R model is gaining increasingly wider use in academic research and in the industrial design of new waterborne products,[45,46] our results highlight the necessity of also considering the effects of salt content and cooperative diffusion.

Acknowledgment. This work was partly funded by the European Commission under Contract IP 011844-2 (NAPOLEON). We gratefully acknowledge helpful discussions with Peter McDonald (University of Surrey) and Ola Karlsson (Lund University). We thank Raquel Rodriguez and Maria Barandarian (University of the Basque Country, San Sebastian) for preparing the latex.

Appendix A: Calculation of the Flow Rate from $\varphi_w(z, t)$

For the experiments reported here, the calculation of the flow rate, J, entails a complication because these samples did experience lateral flow (that is, the coffee-stain effect). Material was moving laterally. The time derivative of the amount of water in the observation volume (the zeroth moment of $\varphi_w(z)$) has two contributions, which are evaporation and laterally diverging flow due to the coffee-stain effect. We have

$$\frac{dm_{0,w}}{dt} = -E - \bar{\varphi}_w \vec{H}_\perp \cdot \vec{v}_\perp \tag{16}$$

where E is the evaporation rate, $\bar{\varphi}_w$ is the vertically averaged water content, $\vec{v}$ is the vertically averaged lateral speed of motion, and the index $\perp$ denotes in-plane directions (x and y). The decrease of the total amount of polymer has only one source, which is the diverging flow. We have

$$\frac{d}{dt} m_{0,pol} = \frac{d}{dt}(H - m_{0,w}) = -\bar{\varphi}_{pol} H \vec{\nabla}_\perp \cdot \vec{v}_\perp = -(1 - \bar{\varphi}_w) H \vec{\nabla}_\perp \cdot \vec{v}_\perp \tag{17}$$

In the two equations above, we have assumed the speed $\vec{v}$ to be about the same for water and the polymer. From eqs 16 and 17, we obtain the evaporation rate as

$$\begin{aligned} E &= -\frac{dm_{0,w}}{dt} - \bar{\varphi}_w H \vec{\nabla}_\perp \cdot \vec{v}_\perp \\ &= -\frac{dm_{0,w}}{dt} + \frac{\bar{\varphi}_w}{(1 - \bar{\varphi}_w)} \frac{d}{dt}(H - m_{0,w}) \\ &= -\frac{1}{(1 - \bar{\varphi}_w)} \frac{dm_{0,w}}{dt} + \frac{\bar{\varphi}_w}{(1 - \bar{\varphi}_w)} \frac{dH}{dt} \end{aligned} \tag{18}$$

In the absence of the coffee-stain effect, dH/dt is equal to d$m_{0,w}$/dt and the evaporation rate is the same as the time derivative of the zeroth moment. The flow rate close to the top of the film is given by

$$\frac{J_w}{\rho_w} \sim E - \varphi_w(H) \frac{dH}{dt} \tag{19}$$

where ρ_w is the density of water. Inserting eq 18 into eq 19 yields

$$\frac{J_w}{\rho_w} = -\frac{1}{(1-\bar{\varphi}_w)}\frac{dm_{0,w}}{dt} + \left(\frac{\bar{\varphi}_w}{(1-\bar{\varphi}_w)} - \varphi_w(H)\right)\frac{dH}{dt} \quad (20)$$

Appendix B: On Cooperative Diffusion

For densely packed systems, the equilibration of concentration gradients primarily happens via a cascade of interparticle collisions. The individual particles only move by small amounts. They stay within their local cages. The entire ensemble rearranges such that the concentration is the same everywhere after equilibration.[40–42] Clearly, this kind of cooperative motion is important in colloidal dispersions with a solids content of about 50 vol % or more. Below, we go through the algebraic derivation of eq 6 and compare to ref 16.

On a fundamental level, Fick's first law states that material flow is coupled to gradients in the chemical potential:

$$J_2 = -D_0 K\frac{c_2}{RT}\nabla\mu_2 = -D_0 K\frac{1}{RT}\frac{3}{4\pi a^3 N_A}\varphi_2\nabla\mu_2 \quad (21)$$

Here, J is the flow, D_0 is the Stokes−Einstein diffusivity, K is the sedimentation coefficient, c is the particle concentration in moles per unit volume, μ is the chemical potential, a is the particle radius, and φ is the volume fraction. The subscript 2 refers to the solute. At this level, we treat the particles as the solute. For binary, incompressible mixtures, the Gibbs−Duhem relation says

$$\nabla\mu_2 = -\frac{c_1}{c_2}\nabla\mu_1 = -\frac{\varphi_1}{\bar{V}_1}\frac{N_A 4\pi a^3}{3\varphi_2}\nabla\mu_1 = \frac{\varphi_1}{\varphi_2}\frac{N_A 4\pi a^3}{3}\nabla\Pi \quad (22)$$

The subscript 1 indicates the solvent. $\bar{V}_1$ is the molar volume of the solvent. The osmotic pressure obeys $\nabla\Pi = -\nabla\mu_1/\bar{V}_1$. Inserting eq 22 into eq 21 yields

$$J_2 = -D_0 K\frac{\varphi_1}{RT}\nabla\Pi = -D_0 K\frac{\varphi_1}{RT}\frac{d\Pi}{d\varphi_2}\frac{d\varphi_2}{dc_2}\nabla c_2 = -D_0 K\frac{\varphi_1}{k_B T}\frac{d\Pi}{d\varphi_2}\frac{4\pi a^3}{3}\nabla c_2 \quad (23)$$

For noninteracting systems at high dilution, we have $\varphi_1 \sim 1$, K ~ 1, and $\Pi \sim RTc_2 = k_B T\varphi_2/(4\pi a^3/3)$. In this limit, one recovers $D_{coop} \sim D_0$. Replacing φ_2 by Φ and φ_1 by $(1-\Phi)$ (matching the terminology in the main text) and further identifying the rhs with $-D_{coop}\nabla c_2$ produces eq 6. Equation 2 in ref 32 is missing the term $(1-\Phi)$ because these authors consider the case of $(1-\Phi) \sim 1$. Note that $(1-\Phi) \sim 1$ by no means implies negligible interaction.

Technically speaking, a colloidal dispersion is not a binary mixture, since the serum is not pure water. For the purpose of this calculation, we assume that all molecules dissolved in the serum remain equilibrated with regard to concentration gradients. Deviations from this assumption are known to occur in the late stages of drying, where transport occurs through narrow water channels and additives, such as surfactant, are enriched at the surface.[43] However, the diffusion of any small molecules may be assumed to be much faster than the diffusion of the particles during stage I of the film formation process. With a serum of uniform composition, the dispersion may be treated as a binary system.

Reference 16 contains a model of particle diffusion, which takes interactions into account via the compressibility factor, Z. Z is defined as

$$Z = \frac{\Pi}{RTc_2} \quad (24)$$

$Z = 1$ implies an osmotic pressure of entirely entropic origin. Interparticle forces lead to an enthalpic contribution to the osmotic pressure, and, as a consequence, to a nontrivial $Z(\Phi)$. Unless the sample is dilute, $Z(\Phi)$ must at least account for the excluded volume in order avoid unphysical results. Reference 16 uses $Z = 1/(\Phi_m - \Phi)$, with Φ_m being the maximum packing density of undeformed spheres. As required, Π diverges at $\Phi \sim \Phi_m$. This choice of $Z(\Phi)$ amounts to a simple representation of a hard-sphere fluid (see also ref 37). Reference 16 considers cooperative diffusion via the compressibility factor, even though the term D_{coop} is not explicitly used.

We differ from ref 16 in two respects: First, we lump the effects of cooperative motion into the definition of the Peclet number. The thus-defined Pe is more predictive with regard to skin formation. The difference in the two definitions can easily amount to a difference of a decade in the Pe values. Second, Z as used in our work encompasses electrostatic and van der Waals interactions. In the language of ref 16 we would write

$$Z = \frac{1}{k_B T}\frac{4\pi a^3}{3}\left[\frac{\sqrt{6}}{A_h}(F_{ES}(D) + F_A(D)) + p_{entr}\right] \quad (25)$$

Following refs 32 and 37, we have lumped the excluded volume contribution into p_{entr}, although excluded volume implies repulsive interaction and therefore might be considered to be of enthalpic origin, in principle. The contribution is small compared to the electrostatic and the van der Waals contribution, anyway. Using eq 25 for Z, the simulations described in ref 16 should reproduce our experiments.

Appendix C: Relation between $\bar{\lambda}$ and Drying Rate for Strongly Coupled Elastic Networks

We start out from eq 85 in ref 8, which states that

$$\Phi = \frac{\Phi_{RCP}}{1-\varepsilon} \quad (26)$$

ε is a volume-averaged strain. Rearranging and taking the time derivative yields

$$\frac{\partial\varepsilon}{\partial t} = \frac{\Phi_{RCP}}{\Phi^2}\frac{\partial\Phi}{\partial t} \quad (27)$$

At times where the spheres densely packed, the water distribution again is rather homogeneous and one can use $\Phi \sim \langle\Phi\rangle$. Equation 84 in ref 8 (note the erratum[44]) relates the strain rate, $\partial\varepsilon/\partial t$, to $\bar{\lambda}$ via

$$\frac{\partial\varepsilon}{\partial\bar{t}} = \frac{7}{5}\frac{\bar{\gamma}}{\bar{\lambda}} \quad (28)$$

where $\bar{t} = tE/H$ is a rescaled time. We approximate E/H by the inverse total time of drying, τ_{dry} (cf. eq 13). The parameter $\bar{\gamma}$ is the ratio of the particle/water interface tension to the air/water interface tension. Inserting and rearranging yields (cf. eq 15)

$$\bar{\lambda} = \frac{7}{5}\frac{\bar{\gamma}\langle\Phi\rangle^2}{\Phi_{RCP}\tau_{dry}}\left(\frac{\partial\Phi}{\partial t}\right)^{-1} \quad (29)$$

LA800525N

(40) Batchelor, G. K. *J. Fluid Mech.* **1976**, *74*, 1–29.
(41) Russel, W. B.; Glendinning, A. B. *J. Chem. Phys.* **1981**, *74*, 948–952.
(42) Wang, C. H. *J. Chem. Phys.* **1991**, *95*, 3788–3797.
(43) Juhue, D.; Wang, Y. C.; Lang, J.; Leung, O. M.; Goh, M. C.; Winnik, M. A. *J. Polym. Sci., Part B: Polym. Phys.* **1995**, *33*, 1123–1133.
(44) Routh, A. F.; Russel, W. B. *Langmuir* **2001**, *17*, 7446–7447.
(45) Keddie, J. L.; Mallégol, J.; Dupont, O. *Mater. World* **2001**, *9*(11), 22–24.
(46) Ludwig, I.; Schabel, W.; Kind, M.; Castaing, J.-C.; Ferlin, P. *AIChE J.* **2007**, *53*, 549–560.